Molecular self-organization in cylindrical nanocavities

S. G. Cloutier,* J. N. Eakin, R. S. Guico, M. E. Sousa, G. P. Crawford, and J. M. Xu
Division of Engineering and Department of Physics, Brown University, Providence, Rhode Island 02912, USA
(Received 16 May 2005; revised manuscript received 1 March 2006; published 10 May 2006)

We studied molecular organization in cylindrical nanocavities using liquid crystals. NMR analysis shows high surface-induced ordering way above the bulk critical temperature. The surface-order evolution reveals replacement of the isotropic phase by a paranematic phase and surface-induced disordering in the nematic phase. Due to strong surface potential and nanoconfinement, complete wetting and continuous evolution of the surface-order parameter are observed through the nematic-paranematic transition. As we show, the counter-intuitive absence of complete phase transition at the interface while an abrupt phase transition was measured in the averaged order parameter is in good agreement with established theories.

DOI: 10.1103/PhysRevE.73.051703 PACS number(s): 64.70.Nd, 61.30.Hn, 61.30.Gd, 61.30.Eb

I. INTRODUCTION

Surface-induced self-organization is of great interest in molecular sciences and device applications [1–3]. In nanoscopic systems, it is clear that molecules can self-organize into various phases due to strong molecule-surface interactions and confinement effects, which could enable new potential applications. Under such conditions, one may expect interesting molecular self-organization behaviors unobservable in bulk or microconfined systems.

In liquid crystal systems, it is well established that surface alignment produces orientational ordering at the solid-liquid crystal interface that propagates by elastic forces into the bulk [3,4]. Strong surface-induced effects through confinement also found many practical applications mostly in polymer-dispersed liquid crystal based systems [5–8], where small but finite phase ordering at temperatures above the bulk nematic-isotropic transition point (T_{NI}) was reported for liquid crystal molecules spatially confined into sufficiently small spherical cavities [9,10].

Predicted earlier by Sheng [11,12], this intermediate paranematic phase is principally attributed to surface-induced ordering [11–14]. More recent studies used cylindrical cavities as confining structures since it makes the Deuterium-NMR (^{2}H-NMR) analysis of the system simpler [15–21]. Two principal candidates for cylindrical confinement were the commercial Nuclepore and the Anopore membranes [18,19]. The Nuclepore nonuniform pore diameters range from 15 nm up to 12 μm, such a broad pore-size distribution producing strong NMR-signal averaging. The Anopore has uniform 200 nm-diameter pores [15], which limits confinement effects since most significant departure from the bulk behavior are expected for films with a critical thickness well under 200 nm [12,22].

In this work, we use the well-documented deuterated-5CB liquid crystal to observe the spectral signatures of the nanoconfined molecular organization using ^{2}H-NMR spectroscopy. An anodic aluminum oxide (AAO) membrane with highly uniform periodically distributed cylindrical pores of 25 nm radius was employed as the confining template. The alumina membranes are fabricated in the two-step aluminum anodization process in oxalic electrolyte described previously [23–25]. The resultant nanopore array, grown to a 80 ± 5 μm thickness, features both 105 ± 5 nm lattice-constant and a narrow 25.5 ± 1.5 nm pore-radius distribution, as shown in Fig. 1. Due to its small pore diameter and high degrees of uniformity and ordering, this template offers a unique platform to investigate confined liquid crystals using ^{2}H-NMR. Under such conditions, surface interactions become significant and exciting surface-induced behaviors have been anticipated [11,12,16,17].

II. EXPERIMENTAL METHODS

A. The nematic phase

The well-understood 5CB (4'-pentyl-4-cyanobiphenyl) liquid crystal molecule deuterated in the α-position on the hydrocarbon chain (αd_2-5CB) was used for the experiments [15–17,26,27]. The ^{2}H-NMR spectroscopy measurements on bulk αd_2-5CB liquid crystal in the nematic phase generates a quadrupole frequency splitting $\delta\nu$ directly proportional to the degree of orientational order of the deuterated C-D

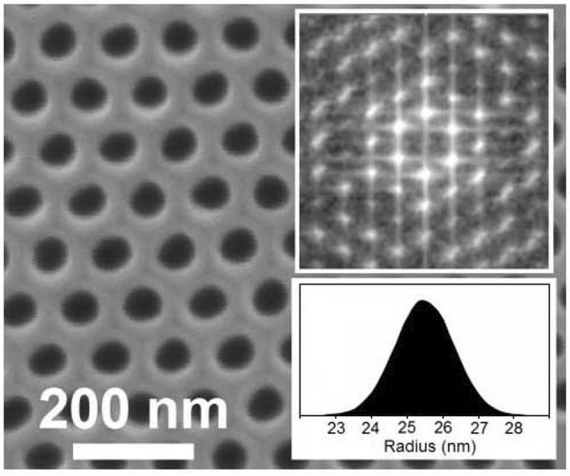

FIG. 1. AAO nanopore array top surface observed using SEM. The insets show the fast-Fourier transform analysis of the periodic nanopore structure and the pore-radius distribution.

*Email address: Sylvain_Cloutier@brown.edu

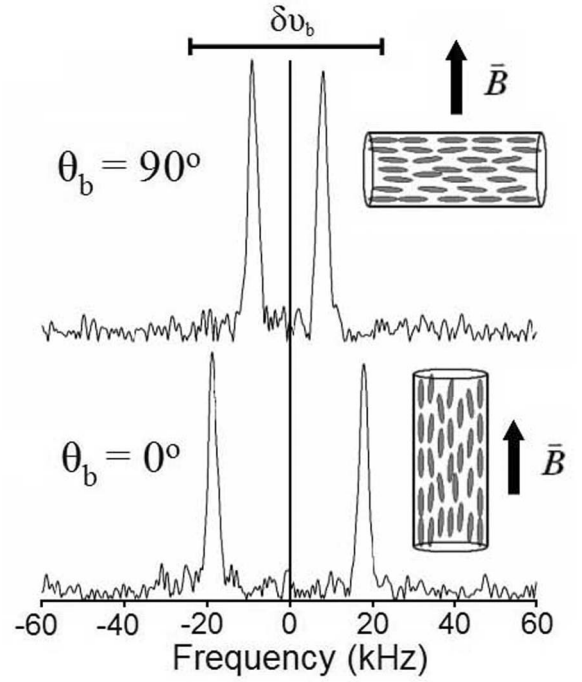

FIG. 2. ^{2}H-NMR spectra with the nanopores axis oriented, respectively, parallel and perpendicular (θ_b=0° and 90°) with respect to the $\vec{B}$ field at $T-T_{NI}=-5$ K and comparison with the bulk quadrupole frequency splitting $\delta\nu_b$.

bond with respect to the static magnetic field $\vec{B}$ [15]. The ^{2}H-NMR quadrupole frequency splitting for confined systems at temperatures below the nematic-isotropic phase-transition temperature (T_{NI}) is described by [28,29]

$$\delta\nu = \frac{S}{S_b}\delta\nu_b\left[\frac{3}{2}\cos^2(\theta)-\frac{1}{2}\right], \qquad (1)$$

where S_b and $\delta\nu_b$ are, respectively, the orientational order parameter and the quadrupole frequency splitting for bulk liquid crystal, and where S and θ are, respectively, the order parameter and the angle between the liquid crystal director $\hat{n}$ and the applied magnetic field $\vec{B}$ for the confined system. This expression assumes an asymmetry parameter equal to zero, which is always the case for bulk uniaxial liquid crystals, but not necessarily for confined systems [30]. However, this effect is predicted to be small and can be safely neglected in most cases [31]. Indeed, experimental results presented in Fig. 2 justify this approximation, since a nonzero asymmetry (or biaxiality) would generate clear signatures in the ^{2}H-NMR spectra [30,32], which were not observed in our system.

Moreover, measurements on such confined system in the nematic phase ($T<T_{NI}$) provide a good indication of the molecular organization inside the cylindrical cavities. The simplest way to access that information is by monitoring the ^{2}H-NMR spectra for the liquid crystal-filled nanopores when the sample is rotated with respect to the $\vec{B}$ field. From the results shown in Fig. 2, one can directly confirm the molecular orientation distribution in the nanopores since $\delta\nu \approx \delta\nu_b$ for θ_b=0° and $\delta\nu \approx \delta\nu_b/2$ for θ_b=90° as predicted by Eq. (1). These results confirm a preferred molecular orientation parallel to the cylindrical pores axis, as shown in the insets of Fig. 2 [15–17].

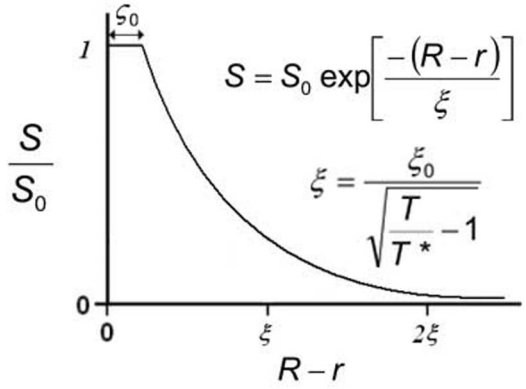

FIG. 3. Spatial distribution of the order parameter S as a function of the radial distance to the nanopore interface at $T>T_{NI}$. Due to surface interactions, there is a residual strongly anchored molecular layer at the interface with a finite thickness ζ_0 between 1.0 and 2.0 nm. Through elastic forces, this surface-*pinned* molecular layer induces ordering even way above T_{NI}. This surface-induced order parameter decays exponentially when moving away from the pore surface, giving rise to a partial ordering.

B. The paranematic phase

When the temperature is raised over T_{NI}, the order parameter inside the cavity can be described as a decaying exponential $S(r)=S_0\exp\left(-\frac{R-r}{\xi}\right)$ where r and R are, respectively, the radial position and the radius of the cylindrical cavity (such that the difference $R-r$ represents the distance to the wall), S_0 is the orientational order parameter at the interface and ξ is the correlation length [15,17,21,33]. The temperature-dependent correlation length is described by Landau-de Gennes (LdG) theory as $\xi=\xi_0\left(\frac{T}{T^*}-1\right)^{-\alpha}$ [15,17]. For the 5CB liquid crystal, ξ_0=0.65 nm, α=1/2 and the second-order transition temperature $T^*=T_{NI}-1.1$ K [15,17,26,27].

This paranematic ordering originates from a thin surface-*pinned* molecular layer with a uniform surface order parameter S_0 due to strong surface anchoring, which induces bulk alignment through short-range elastic interactions explained by the short correlation length above the transition point [12,17,20,21]. The finite thickness ζ_0 of this strongly anchored molecular layer is expected to be between 1.0 and 2.0 nm, depending on the surface energy. The typical spatial distribution of the order parameter $S(r)$ in the paranematic phase is shown in Fig. 3.

The presence of such surface-induced ordering can lead to a residual quadrupolar frequency splitting even at temperatures well above T_{NI}. However, this effect is expected to be small in weakly confined systems [15]. From the previous expression, the correlation length ξ for 5CB corresponds to $\approx$11 nm at T_{NI}, and diminishes to less than 3.5 nm

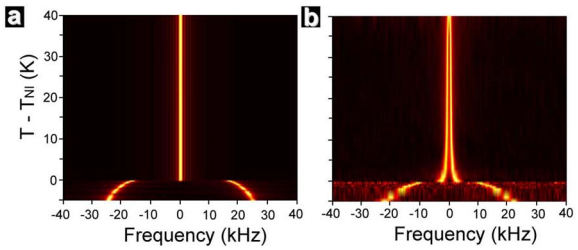

FIG. 4. (Color online) ^{2}H-NMR spectra temperature evolution for (a) bulk and (b) nanoconfined αd_2-5CB.

at temperatures more than 10 K above T_{NI}, which suggests that the surface-induced ordering would indeed be significant only very close to the interface due to short-range elastic interactions.

Figure 4 compares the temperature evolutions of the measured ^{2}H-NMR spectrum for the nanoconfined and bulk liquid crystal systems. As shown in Fig. 5, a large residual quadrupole frequency splitting persisted at temperatures well above T_{NI}, a direct indicator of strong surface-induced ordering associated with a paranematic phase. This residual frequency splitting can be related to the surface-order parameter S_0 by the following relation [15,18]:

$$\langle \delta\nu \rangle = \left(\frac{\delta\nu_b}{S_b} \right) \langle S \rangle = \left(\frac{\delta\nu_b}{S_b} \right) \left(\frac{2S_0\xi}{R} \right), \tag{2}$$

where the brackets indicate a complete spatial averaging effect due to molecular self-diffusion mechanisms. Such an averaging effect can be explained in terms of the characteristic length of diffusion $x_o \approx \sqrt{D/\delta\nu}$, where $D \approx 10^{-11}$ m^2/sec for 5CB, being comparable to the cavity radius R at temperatures above T_{NI} ($x_o > 25$ nm for $T - T_{NI} > 3$ K) [15]. The right side of Eq. (2) also relies on the approximation that $R \gg \xi$, as shown previously for $T > T_{NI}$. As Eq. (2) shows, the combined small radius and high degree of uniformity of the AAO nanopores allows clear measurement of the surface interactions since the quadrupolar frequency splitting is proportional to 1/R and the associated signal averaging over a given pore-diameter distribution is

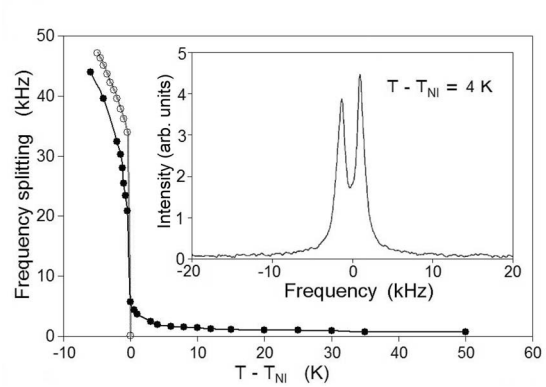

FIG. 5. ^{2}H-NMR quadrupolar frequency splitting temperature evolutions for nanoconfined (•) and bulk (◦) αd_2-5CB. The inset shows the ^{2}H-NMR spectrum for the confined system at 4 K above T_{NI}.

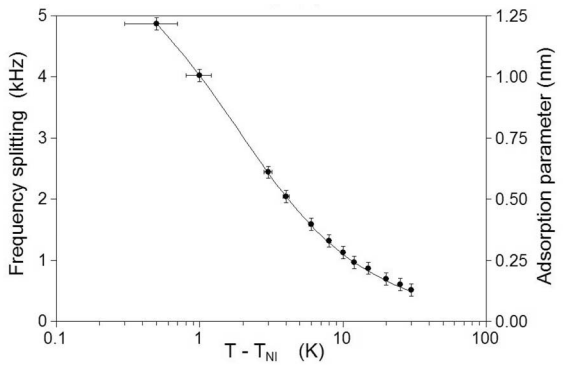

FIG. 6. Paranematic ^{2}H-NMR quadrupolar frequency splitting $\langle \delta\nu \rangle$ and the associated surface adsorption parameter Γ as a function of temperature. The solid line shows the fitting of the data using Eq. (3).

minimized, making the AAO template an efficient platform to investigate such surface-induced molecular organization.

The averaged order parameter $\langle S \rangle$ for the nanoconfined system can be obtained directly from the ^{2}H-NMR nematic and paranematic frequency splitting $\langle \delta\nu \rangle$ measurements using Eqs. (1) and (2), respectively.

III. RESULTS AND DISCUSSION

A. Paranematic ordering and surface adsorption

The paranematic frequency-splitting temperature evolution is highlighted in Fig. 6. The associated surface adsorption Γ is obtained directly from the frequency splitting since $\Gamma = \frac{R}{2} \frac{\langle \delta\nu \rangle}{\delta\nu_o}$ for a parallel axial distribution where $\delta\nu_o \approx 50$ kHz [17]. Just above T_{NI}, large quadrupole frequency splittings were measured, suggesting degrees of ordering far larger than those reported in other microconfined systems [16,17].

The weak logarithmic divergence in Fig. 6 suggests a complete molecular wetting regime [16,17]. To the authors' knowledge, complete orientational wetting has not been previously observed in confined systems [16,17,28,29]. Surface wetting is known to depend on the surface adsorption parameter [3]. Since the surface adsorption is directly proportional to the NMR splitting and therefore inversely proportional to the cavity size R, surface wetting should indeed be favored in such nanoconfined systems.

B. Paranematic surface order parameter

From the experimental data shown in Fig. 6, one can also directly obtain the temperature-independent S_{00} surface-order coefficient from LdG theory and the corresponding surface-*pinned* molecular-layer effective thickness ζ_0 by fitting the temperature dependence of $\langle \delta\nu \rangle$ using the following equation [18]:

$$\langle \delta\nu \rangle = \left(\frac{\delta\nu_b}{S_b} \right) \left(\frac{2S_{00}}{R} \right) \left[\frac{\xi_0}{\frac{T}{T^*} - 1} + \frac{\zeta_0}{\sqrt{\frac{T}{T^*} - 1}} \right] \tag{3}$$

by using the second-order transition temperature $T^* = T_{NI} - \beta$, $\delta\nu_b/S_b \approx 48$, $\xi_0 = 0.65$ nm, and $R \approx 25$ nm [18].

The optimal fitting shown in Fig. 6 yields $S_{00}=0.0135\pm0.001$, $\beta=1.5\pm0.1$ K, and $\zeta_0=1.73\pm0.15$ nm, in good agreement with previous reports [15–17]. Moreover, the transition-temperature T_{NI} appears to be slightly higher due to confinement, as suggested by the increased β obtained from the fit ($\beta\approx1.5$ K for the confined system and $\beta\approx1.1$ K for the bulk) [29], also in good agreement with theoretical expectations [12,22] and numerical simulations [34].

Therefore, the positive surface-order parameter S_0 can be directly obtained at any given paranematic temperature using the expression [18]

$$S_0 = S_{00}\left(\frac{T}{T^*}-1\right)^{-1/2} \tag{4}$$

with the known entities $S_{00}=0.0135\pm0.001$ and $T^*=T_{NI}^{bulk}-1.5$ K.

C. Nematic surface order parameter

Another interesting phenomenon stems from the quadrupole frequency splitting comparison of the confined and bulk systems displayed in Fig. 5. In the nematic phase, the confined system shows a quadrupole frequency splitting noticeably weaker than the bulk. With $T>T_{NI}$, we demonstrated that surface interactions induce a significant degree of ordering in the isotropic phase by surface-pinning. From similar reasoning, when $T<T_{NI}$, surface interactions can introduce a finite degree of *disordering* in the bulk nematic distribution [14,35–37]. This surface-induced disordering decays exponentially when moving away from the pore surface, giving rise to an averaged order parameter observed in the ^{2}H-NMR smaller than the bulk order parameter S_b. Far from the surface, volume effects dominate and the order parameter is equal to the bulk [37].

A phenomenological way to model this surface-induced disordering is to describe the local order parameter as

$$S(r) = S_b - (S_b - S_0)\exp\left(-\frac{R-r}{\xi}\right), \tag{5}$$

where S_b is the bulk order parameter and the exponential term would be the surface-induced disorder with ξ the correlation length [14,37]. As shown in Fig. 7, this expression simply represents an inverted exponential with an order parameter $S\rightarrow S_0$ close to the interface (when $R-r\ll\xi$) and an order parameter $S\rightarrow S_b$ when $R-r\gg\xi$ [37].

In such nanoconfined systems, one also measures the ^{2}H-NMR frequency splitting due to the averaged order parameter, even in the nematic phase. Such an assumption is justified considering the diffusion length $x_o\approx\sqrt{10^{-11}/\delta\nu}$ being comparable to the cavity radius R even in the nematic phase ($x_o\approx22$ nm for $T-T_{NI}=-0.5$ K and $x_o\approx15$ nm for $T-T_{NI}=-5$ K). By using Eq. (5), the averaged order parameter can be described as

$$\langle S\rangle = \frac{\int rS(r)dr}{\int rdr} = S_b - \left(\frac{2\xi}{R}\right)[S_b - S_0]. \tag{6}$$

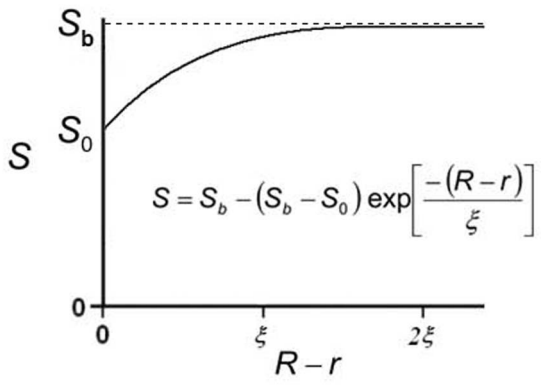

FIG. 7. Spatial distribution of the order parameter S as a function of the radial distance to the interface at $T<T_{NI}$ [37]. Due to surface interactions, there is a surface-induced disordering that prevails close to the surface.

However, Eq. (6) assumes that $R>\xi$. In such a case, the surface-order parameter can only be observed for pore dimensions comparable to the coherence length, since $\langle S\rangle\approx S_b$ for large cavities ($R\gg\xi$) and any surface-order information becomes unaccessible [16,17,28,29]. Clearly, this expression does not apply to our system since the nematic correlation length is expected to be relatively large when $T<T_{NI}$ [27,33]. Considering the nanometer scale cavity radius R, we can safely assume that the correlation length is much longer than the pore radius ($\xi\gg R$) such that surface effects dominate and the order parameter $S(r)$ is equal to the surface-order parameter S_0 everywhere in the cavity, as predicted by Eq. (5). As a consequence, the averaged order parameter $\langle S\rangle$ obtained directly from the ^{2}H-NMR quadrupolar frequency splitting measured in the nematic phase ($T<T_{NI}$) is equal to the surface-order parameter S_0.

D. Averaged and surface order parameters phase transitions

As we have shown, the temperature evolutions for the confined surface-order parameter S_0 and averaged order parameter $\langle S\rangle$ can be obtained directly from the ^{2}H-NMR spectra temperature evolution. The bulk order parameter S_b temperature evolution was also obtained from the bulk αd_2-5CB liquid crystal frequency splitting [18], which measurement is consistent with previous literature reports [38].

Figure 8 displays the continuous nanoconfined surface-order parameter S_0 evolution from the nematic phase ($T-T_{NI}=-5$ K) up to deep into the paranematic phase ($T-T_{NI}=30$ K). Figure 9 shows the discontinuous averaged order parameter $\langle S\rangle$ evolution, proportional to the measured frequency splitting. The bulk order parameter S_b temperature evolution is also displayed for comparison.

The combined strong orientational surface wetting and the continuous evolution of S_0 through the bulk nematic-isotropic phase transition shown in Fig. 8 requires both a strong surface potential G/A and nanoconfinement [12,14]. The surface potential can be obtained directly from the

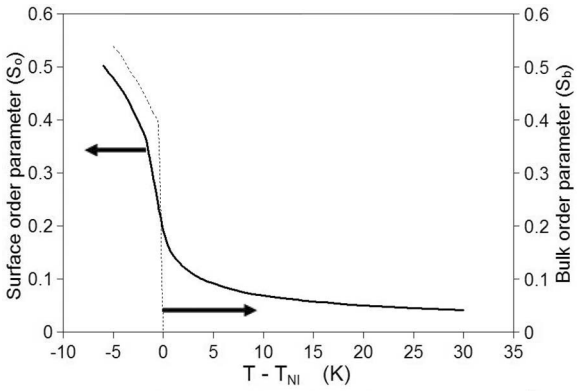

FIG. 8. Surface order parameter S_0 from the nanoconfined system (plain line) in both the nematic ($T<T_{NI}$) and the paranematic ($T>T_{NI}$) phases. The bulk order parameter S_b (dotted line) is displayed as a comparison.

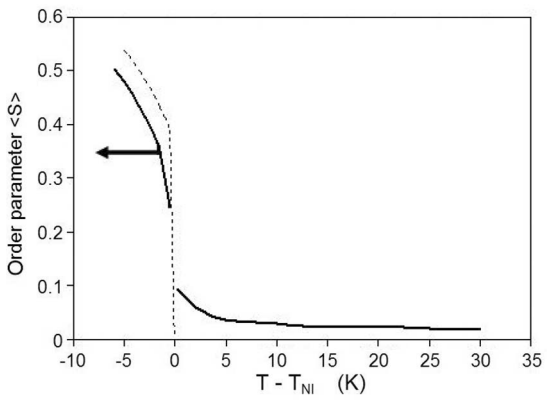

FIG. 9. Averaged order parameter $\langle S\rangle$ temperature evolution for the confined system. The bulk order parameter S_b (dotted line) is also displayed as a comparison.

temperature-independent surface-order parameter since $G/A=S_{00}\sqrt{aLT^*}=(3.54\pm0.25)10^{-4}$ J/m^2 where a, L, and T^* are material-dependent parameters known for 5CB [12,29]. Therefore, the associated dimensionless substrate potential $g=S_{00}=0.0135$ [12,29].

According to theory, three possible phase-transition regimes are possible for surface-ordered liquid crystal systems [12]. Those three phase-transition regimes are described in Table I.

For the cases shown in Table I (a) and (b), the surface potential is either too small ($g<0.012$) or the film thickness parameter is too large ($R/\xi_0>65$) for the surface energy to compete with the volume energy, leading to a bulk-like behavior where both the surface-order parameter S_0 and the averaged order parameter $\langle S\rangle$ display a discontinuity in their temperature evolution associated with phase transition [12].

When the dimensionless substrate potential $g>0.012$ and the film thickness is sufficiently small ($R/\xi_0<65$), corresponding to the cases shown in Table I (c) and (d), the surface-order parameter S_0 temperature evolution becomes continuous due to the absence of complete phase transition at the interface originating from the strong surface potential [12,14]. In such a regime, the averaged order parameter $\langle S\rangle$ will show a discontinuous temperature evolution associated with phase transition only if the critical thickness parameter $R/\xi_o>26$ ($R>16$ nm for 5CB), and becomes continuous otherwise due to a dominating surface energy [12,22].

In our case, we have shown experimentally that $g\approx0.0135$ and $R/\xi_o\approx38$, corresponding to the case shown in Table I(c). Therefore, the order parameters temperature evolution in our nanoconfined system show a unique molecular state with no complete orientational-phase transition at the interface (S_0) but an abrupt discontinuity associated with phase transition for the averaged order parameter $\langle S\rangle$, in perfect agreement with theoretical predictions by Sheng [12]. To the best of our knowledge, this unique molecular organization phase theoretically predicted more than two decades ago has never been reported before, most likely due to the difficulty to obtain a porous nanopore template offering both the small pore diameter and the high pore-diameter uniformity enabled by the anodic aluminum oxide (AAO) nanopore array.

Moreover, the measured $S_0\approx0.2$ at T_{NI} for $g>0.012$ and $R/\xi_o\approx38$ is consistent with theoretical predictions [12]. The transition-temperature T_{NI} was slightly increased due to confinement, as suggested by the increased β obtained by fitting the experimental results ($\beta\approx1.5$ K for the confined system and $\beta\approx1.1$ K for the bulk) [29], also in good agreement with theoretical expectations [12,22] and numerical simulations [34].

Figure 10 displays the nanoconfined order parameter S spatial distribution temperature evolution from the nematic phase ($T-T_{NI}=-5$ K) up to deep into the paranematic phase ($T-T_{NI}=30$ K). The spatial distribution evolution is reconstructed using the surface-order parameter, correlation lengths, and the surface-pinned molecular layer thickness obtained from the ^{2}H-NMR temperature-evolution measurements. Below the second-order transition temperature (T^*), the correlation length is infinite and the order parameter is constant everywhere in the pore. Above T^*, the ordering decays exponentially when moving away from the pore surface. However, there is a residual strongly anchored molecular layer at the interface with a finite thickness ζ_0 between

TABLE I. Possible phase-transition regimes predicted for surface-aligned liquid crystal systems [12].

	(*a*)	(*b*)	(*c*)	(*d*)
g	<0.012	>0.012	>0.012	>0.012
R/ξ_0	Independent	>65	26–65	<26
$\langle S\rangle$	Discontinuous	Discontinuous	Discontinuous	Continuous
S_0	Discontinuous	Discontinuous	Continuous	Continuous

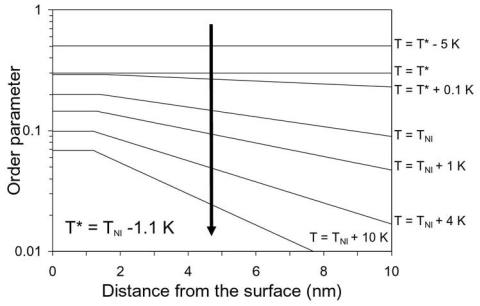

FIG. 10. Spatial distribution of the order parameter $S(r)$ as a function of the radial distance to the nanopore interface. A residual strongly anchored molecular layer at the interface with a finite thickness ζ_0 between 1.0 and 2.0 nm remains up to 30 K above T^* and give rise to the partial ordering observed in the ^{2}H-NMR spectra through short-range elastic interactions.

1.0 and 2.0 nm that remains up to 30 K above T^* and gives rise to the partial ordering observed in the ^{2}H-NMR spectra.

Additional nonclassical effects can also take place in such strongly confined systems. However, even though quenching-disorder effects have been previously observed in confined systems [39,40], our experimental results clearly suggest that such effects did not play a significant role here due to the absence of any "memorylike" behavior. The tricritical exponent term for the nematic-isotropic phase transition could not be observed either [41]. However, it has been clearly established previously that experimental results can lead to great uncertainties on the exact nature of the transition [42], especially in the isotropic phase of nematogens [42,43]. Such discrepancies have been attributed to more subtle effects such as pretransitional fluctuation phenomena [42]. Geometrical factors are also known to play an important role in strongly confined systems since they rely on elastic deformations and strong curvature effects. In the parallel-axial molecular distribution such elastic deformations are small or nonexistent, therefore we can expect no direct influence from the geometrical factors. This assumption was also further justified by the good agreement between experimental results and classical models.

IV. CONCLUSIONS

In summary, we studied molecular self-organization in a nanoconfined system using ^{2}H-NMR spectroscopy of α-deuterated 5CB liquid crystal. We found that the confined molecular organization in the nematic phase follows a parallel axial distribution. A model was presented to extract the surface-order parameter in both the nematic and the paranematic phases from the ^{2}H-NMR spectrum temperature evolution. The quadrupole frequency splitting observed up to 50 K above the bulk nematic-isotropic transition temperature (T_{NI}) demonstrates the existence of a 1.7 nm-thick surface-*pinned* molecular layer at the solid-liquid crystal interface. The orientational surface-order coefficient (S_{00}) indicates a high degree of paranematic ordering in comparison with previous reports using bulk and micro-confined systems [15–17]. The high surface potential ($3.54 \cdot 10^{-4}$ J/m^2) and nanoconfinement that lead to such strong surface-induced order deep in the bulk isotropic phase also lead to a finite degree of surface-induced disorder in the nematic phase. A unique surface-induced molecular phase with a complete orientational wetting regime as well as a continuous surface-order (S_0) and discontinuous averaged order-parameter $\langle S \rangle$ evolution through the nematic-paranematic transition were observed, as theoretically predicted for molecular films with a thickness ($\approx R$) between 16 and 43 nm combined with a high surface potential [12]. This capacity to control and preserve molecular ordering using nanoconfined systems could be useful in a variety of self-organization applications, and helpful in providing insights into the collective behaviors in strongly cooperative molecular systems.

ACKNOWLEDGMENTS

S.G.C. is thankful to NSERC and J.M.X. thanks DARPA, AFOSR, and ONR, for their support, G.P.C. acknowledges NSF DMR-0506072.

[1] B. Bahadur, Mol. Cryst. Liq. Cryst. **109**, 1 (1984).
[2] P. W. Bohn, Annu. Rev. Phys. Chem. **44**, 37 (1993).
[3] L. M. Blinov and V. G. Chigrinov, *Electrooptic Effects in Liquid Crystal Materials* (Springer-Verlag, New York, 1996).
[4] A. Šarlah and S. Žumer, in *Surfaces and Interfaces of Liquid Crystals*, edited by T. Rasing and I. Muševič (Springer, Berlin, 2004), pp. 249–279.
[5] G. P. Crawford and S. Žumer, in *Liquid Crystals in Complex Geometries*, edited by G. P. Crawford and S. Žumer (Taylor & Francis, Bristol, 1996), pp. 1–19.
[6] A. Fuh and T. H. Lin, J. Appl. Phys. **96**, 5402 (2004).
[7] Y. J. Liu, X. W. Sun, H. T. Dai, J. H. Liu, and K. S. Xu, Opt. Mater. (Amsterdam, Neth.) (Amsterdam, Neth.) **27**, 1451 (2005).
[8] I. Amimori, J. N. Eakin, J. Qi, G. Skačej, S. Žumer, and G. P. Crawford, Phys. Rev. E **71**, 031702 (2005).
[9] J. W. Doane, N. A. Vaz, B. G. Wu, and S. Žumer, Appl. Phys. Lett. **48**, 269 (1986).
[10] A. Golemme, S. Žumer, D. W. Allender, and J. W. Doane, Phys. Rev. Lett. **61**, 2937 (1988).
[11] P. Sheng, Phys. Rev. Lett. **37**, 1059 (1976).
[12] P. Sheng, Phys. Rev. A **26**, 1610 (1982).
[13] P. Ziherl and S. Žumer, Phys. Rev. Lett. **78**, 682 (1997).
[14] A. Šarlah and S. Žumer, in *Surfaces and Interfaces of Liquid Crystals*, edited by T. Rasing and I. Muševič (Springer, Berlin, 2004), pp. 211–247.
[15] J. W. Doane and G. P. Crawford, *Encyclopedia of Nuclear Magnetic Resonance* (Wiley, New York, 1995).
[16] G. P. Crawford, R. Ondris-Crawford, S. Žumer, and J. W. Doane, Phys. Rev. Lett. **70**, 1838 (1993).

[17] G. P. Crawford, R. J. Ondris-Crawford, J. W. Doane, and S. Žumer, Phys. Rev. E **53**, 3647 (1996).
[18] G. P. Crawford, M. Vilfan, J. W. Doane, and I. Vilfan, Phys. Rev. A **43**, 835 (1991).
[19] G. P. Crawford, L. M. Steele, R. Ondris-Crawford, G. S. Iannacchione, C. J. Yeager, J. W. Doane, and D. Finotello, J. Chem. Phys. **96**, 7788 (1992).
[20] M. Vilfan, B. Zalar, A. K. Fontecchio, M. Vilfan, M. J. Escuti, G. P. Crawford, and S. Žumer, Phys. Rev. E **66**, 021710 (2002).
[21] M. Vilfan, B. Zalar, G. P. Crawford, D. Finotello, and S. Žumer, in *Surfaces and Interfaces of Liquid Crystals*, edited by T. Rasing and I. Muševič (Springer, Berlin, 2004), pp. 17–40.
[22] F. Batalioto, L. R. Evangelista, and G. Barbero, Phys. Lett. A **324**, 198 (2004).
[23] J. Liang, H. Chik, A. Yin, and J. Xu, J. Appl. Phys. **91**, 2544 (2002).
[24] A. P. Li, F. Müller, A. Birner, K. Nielsch, and U. Gösele, J. Appl. Phys. **84**, 6023 (1998).
[25] H. Masuda, H. Yamada, M. Satoh, H. Asoh, M. Nakao, and T. Tamamura, Appl. Phys. Lett. **71**, 2770 (1997).
[26] H. J. Coles, Mol. Cryst. Liq. Cryst. **49**, 67 (1978).
[27] S. Chandrasekhar, *Liquid Crystals* (Cambridge University Press, London, 1977).
[28] G. P. Crawford, D. K. Yang, S. Žumer, D. Finotello, and J. W. Doane, Phys. Rev. Lett. **66**, 723 (1991).
[29] G. P. Crawford, R. Stannarius, and J. W. Doane, Phys. Rev. A **44**, 2558 (1991).
[30] B. Zalar, S. Žumer, and D. Finotello, Phys. Rev. Lett. **84**, 4866 (2000).
[31] N. Schopohl and T. J. Sluckin, Phys. Rev. Lett. **59**, 2582 (1987).
[32] R. Y. Dong, *Nuclear Magnetic Resonance of Liquid Crystals* (Springer-Verlag, New-York, 1997), 2nd ed.
[33] P. G. de Gennes, *Physics of Liquid Crystals* (Clarendon, Oxford, 1974).
[34] R. M. Marroum, G. S. Iannacchione, D. Finotello, and M. A. Lee, Phys. Rev. E **51**, R2743 (1995).
[35] T. Moses and Y. R. Shen, Phys. Rev. Lett. **67**, 2033 (1991).
[36] P. Ziherl, A. Šarlah, and S. Žumer, Phys. Rev. E **58**, 602 (1998).
[37] G. Barbero and G. Durand, in *Liquid Crystals in Complex Geometries*, edited by G. P. Crawford and S. Žumer (Taylor & Francis, Bristol, 1996), pp. 21–52.
[38] M. Marinelli, F. Mercuri, U. Zammit, and F. Scudieri, Phys. Rev. E **58**, 5860 (1998).
[39] M. Rotunno, M. Buscaglia, C. Chiccoli, F. Mantegazza, P. Pasini, T. Bellini, and C. Zannoni, Phys. Rev. Lett. **94**, 097802 (2005).
[40] R. Bandyopadhyay, D. Liang, R. H. Colby, J. L. Harden, and R. L. Leheny, Phys. Rev. Lett. **94**, 107801 (2005).
[41] P. H. Keyes and J. R. Shane, Phys. Rev. Lett. **42**, 722 (1979).
[42] P. K. Mukherjee, J. Phys.: Condens. Matter **10**, 9191 (1998).
[43] A. D. Drozd-Rzoska, S. J. Rzoska, and J. Ziolo, Phys. Rev. E **54**, 6452 (1996).